Numerical Investigation of Active Flow Control on Laminar Forced Convection over a Backward Facing Step Surrounded by Multiple Jets

U. C. Coskun[†], S. Cadirci and H. Gunes

Department of Mechanical Engineering, Istanbul Technical University (ITU), Istanbul, 34437, Turkey

† *Corresponding Author Email*: *ucoskun@itu.edu.tr*

ABSTRACT

Laminar, transient forced convection problem over a 2D backward facing step (BFS) at an inlet Reynolds number (Re) of 400 is investigated numerically using OpenFOAM. To increase the Nusselt number (Nu) along the bottom wall, active flow control is applied by zero-net-mass-flux (ZNMF) combinations of suction and injection through three thin slits which are placed on the top, step and the bottom walls in the vicinity of the BFS. The combinations of each jet velocity is determined by jet to inlet mean velocity ratios which are limited to integer numbers between -2 and 2 and satisfying ZNMF condition where negative and positive values indicate suction and injection, respectively. All 19 cases which satisfy these rules are investigated. Average Nusselt number, friction coefficient and recirculation zone lengths are calculated along the bottom wall from time averaged flow fields. Among 19 cases with each having different jet configuration, some cases converged to steady state solution while others indicated temporal effects and converged to periodic solutions. To understand these transient effects, velocity oscillation magnitude and Strouhal number which are monitored at a selected critical point are evaluated. It is shown that temporal interaction of chosen active flow control methodology has significant effect on enhancing mixing which results in an increase of Nusselt number. Among all cases, the best case concerning thermal improvement has an increase of 78.5% in Nu number while the best aerodynamic improvement is achieved for another case with a decrease of 81% in total recirculation zone length compared to the reference case where no control is applied.

Keywords: Backward facing step; Active flow control; Open FOAM; Heat transfer enhancement; CFD.

NOMENCLATURE

C_f	friction coefficient		St	Strouhal number
c_p	specific heat		T	temperature
D_H	hydraulic diameter		T_{ref}	inlet temperature
DIC	Diagonal-Based Incomplete Cholesky		T_H	bottom wall temperature
f	frequency		u	x-velocity
FFT	Fast Fourier Transform		U_c	inlet centerline velocity
g	gravitational acceleration		U_m	inlet mean velocity
GAMG	Geometric Agglomerated Algebraic Multigrid		v	y-velocity
			V_j	jet velocity
h	step height		ZNMF	Zero Net Mass Flux
H	total channel height		α	thermal diffusivity
h_{air}	convective heat transfer coefficient of air		β	thermal expansion coefficient
k	thermal conductivity		Δt	time step
Nu	Nusselt number		ΔT	temperature difference
OscMag	Oscillation Magnitude		μ	dynamic viscosity
p	pressure		ν	kinematic viscosity
Pr	Prandtl number		ρ	density
Re	Reynolds number		τ_{Wall}	wall shear stress
RZL	Recirculation Zone Length			

1. INTRODUCTION

Flow over a backward facing step represents similarities to many thermal and aerodynamic engineering applications such as vehicle aerodynamics and cooling of electronic devices. Therefore, many researchers devoted their attention to this problem and investigated it both numerically and experimentally. In such applications, the main goal is to influence drag, postpone or prevent flow separation and enhance heat transfer. Flow control techniques are effective tools to achieve these goals.

Flow control approaches cover a wide range of engineering goals such as prevention or delay of boundary layer separation, delay of transition, noise suppression, drag reduction and mixing enhancement. Flow control strategies can be classified as passive, active or combination of both. While active flow control requires external energy, passive control does not require any energy input [Gad-el Hak (2006)].

Some of the most common active flow control techniques include heating or cooling from the surface, suction and injection into the flow domain by micro localized jets (Ahmed *et al.* (2014), Kanchi and Mashayek (2012)) and macro localized jets (Oyakawa *et al.* (1995), Kiwan (2008), Uruba *et al.* (2007), Emami-Naeini *et al.* (2005)) , wall jets (Nait Bouda *et al.* (2008)), synthetic jets (Xu *et al.* (2015), Takano *et al.* (2014), Okada *et al.* (2010), Dandois *et al.* (2007)), periodic excitations (Mehrez *et al.* (2010a), Mehrez *et al.* (2011), Bouterra *et al.* (2011), Chun and Sung (1996), Kim *et al.* (2007), Rhee and Sung (2000)), perturbations (Okada *et al.* (2010), Kapiris and Mathioulakis (2014), Mehrez *et al.* (2010b), Dejoan *et al.* (2005), Yoshioka *et al.* (2001)), rotating cylinder (Anguraj and Palraj (2018)) and exposing shear layer to acoustic waves (Wengle and Huppertz (2001)). Adding vortex generators of various shapes (Ahmed *et al.* (2018), Kumar and Vengadesan (2018)), changing the channel geometry such as step and upper wall inclination (Bayraktar (2014)) are some examples of passive flow control techniques for hydrodynamic and thermal enhancement.

From the literature, it is known that active flow control is very effective in enhancing heat transfer over a BFS. Velocity pulsation frequency and pressure gradient amplitude at the inlet section of the channel were found to be effective in reducing the reattachment length and enhancing forced convective (Valencia and Hinojosa (1997), Tihon *et al.* (2010), Velazquez *et al.* (2008)) and mixed convective (Khanafer *et al.* (2008), Lin *et al.* (1990)) heat transfer for unsteady, laminar flows over a BFS. Another method to influence the velocity profiles over a BFS flow is the implementation of nanofluids into the base flow and can be used as a control methodology (Al-aswadi *et al.* (2010)).

The experimental and numerical study conducted by Armaly *et al.* (1983) provided an outline for the BFS flows under laminar, transitional and turbulent flow conditions. They stated that a BFS flow remains in the laminar flow regime below $Re_{inlet} = 1200$. They also showed that the flow for $400 < Re < 6000$ was strongly 3D but maintained it's symmetry to the centre plane. In later studies, Biswas *et al.* (2004) and Erturk (2008) repeated the numerical calculations for BFS flows in a wider range of parameters and they also showed that 2D simulations up to $Re = 400$ were in excellent agreement with the experimental measurements of the flow field at the vertical mid plane.

Oyakawa *et al.* (1995) studied turbulent flow over a BFS, experimentally. In their study, they applied local injection from a single slit on the upper wall located downstream of the BFS. They investigated the effects of jet location and jet velocity on the heat transfer, pressure coefficient and recirculation zone length. Uruba *et al.* (2007) conducted an experimental study on turbulent BFS flow and applied local suction and injection from the step foot. They investigated the effects of slit's profile and jet flow rate on recirculation zone length. Zhao and Dong (2020) investigated the impact of step height and wall suction located immediately behind the BFS on oncoming Tollmien-Schlichting waves. They found that for a step with a moderate height, suction with a small flux was sufficient to compensate the destabilizing effect of the step. Chun and Sung (1996) carried out an experimental study on the turbulent BFS flow where they controlled the flow with small localized forcing near the separation edge and investigated the change of the flow separation. Chovet *et al.* (2016), Chovet *et al.* (2019) designed a micro-blower and attached several of these actuators in a row in span-wise direction in the upstream of a turbulent backward facing step with the aim of reducing recirculation zone length by changing forcing frequency.

Li *et al.* (2019) studied an application of active flow control on turbulent flow over a BFS, experimentally. They reduced the recirculation bubble length and improved heat transfer by controlling frequency and amplitude of a single jet placed at the separation point. Kiwan (2008) conducted a numerical study on a turbulent BFS flow and studied the effects of control parameters including the position, angle, flow rate of a single jet placed on the upper wall downstream of the BFS along with inlet Reynolds number and expansion ratio of the channel on reattachment length of separation zones which occur on both upper and lower walls.

Giachetti *et al.* (2018) used multiple array of synthetic jets upstream of the BFS and investigated the effects of jet flow frequency and amplitude on heat transfer under both laminar and turbulent cross flow, experimentally. Velazquez *et al.* (2008)
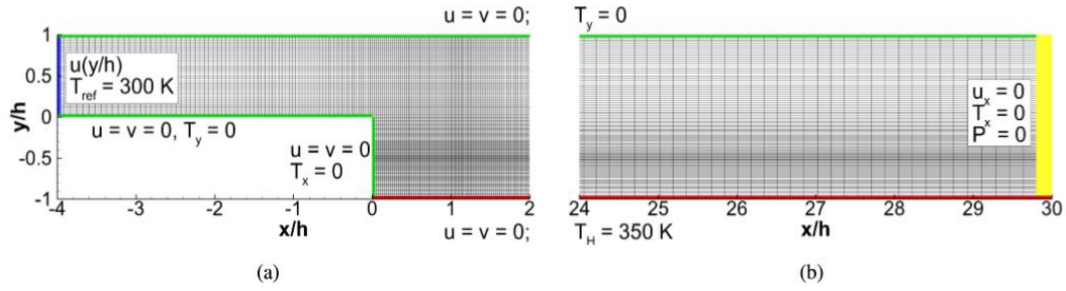
Fig. 1. Computational domain showing the grid distribution with applied boundary conditions: (a) vicinity of the inlet and step, (b) outlet section.

worked on a laminar 2D BFS flow, numerically. They investigated the effects of pulsation frequency and pressure gradient at the channel inlet on the heat transfer from bottom wall. There are several similar experimental and numerical studies on the 3D applicability of the current active flow control method based on uniform actuation in span-wise direction using arrays of micro-jets (Ahmed *et al.* (2014)) or long thin slit at the corner (Yoshioka *et al.* (2001), Chun and Sung (1996), Dandois *et al.* (2007)) or foot (Uruba *et al.* (2007)) of the BFS.

However in literature, most of the active flow control applications on BFS flow such as suction or injection through thin slits, periodic perturbation, acoustic excitation and surface forcing were applied from a single location either on the step or upper wall. The authors did not encounter any study related to the effect of multiple jets surrounding the BFS and their interactions with each other under varying jet flow rates for laminar base flow.

The novelty of this study is to fill the gap in literature of applying active flow control by using multiple actuators at various locations surrounding the BFS. In the current study, 2D, incompressible, laminar air flow over a BFS with an expansion ratio of 2 is investigated numerically. Three thin slits where air can be sucked or injected from at different flow rates are placed on upper, step and lower walls in the vicinity of BFS. All the ZNMF combinations consisting of three jets each having 5 various jet flow rates are simulated. It is shown that certain combinations of studied cases revealed strong transient interaction which significantly improved mixing in the channel resulting in enhanced heat transfer without increasing the friction coefficient.

2. PROBLEM DESCRIPTION

The channel geometry consists of a BFS with a step height h = 0.01 m and a total height H = 2h. The upstream and downstream channel lengths are defined as 4h and 30h, respectively. The working fluid is air with constant thermophysical properties, which are $\mu = 1.81x10-5kg/ms$, $\rho = 1.205kg/m^3$, $cp = 1005J/kgK$, $k = 0.0255W/mK$ and $\alpha = 2.11x10^{-5}m^2/s$.

Inlet Reynolds Number is taken as 400 and its

definition is given in Eq. (1).

$$\text{Re} = \frac{\rho U_m D_H}{\mu} \tag{1}$$

The mean velocity at the channel's inlet is 2/3 of the centreline velocity (U_c) and the hydraulic diameter is equal to twice of the inlet channel height considering this is a 2D channel geometry. The computational domain is shown in Fig.1.

The fully-developed laminar velocity profile is imposed at the inlet of the channel as given in Eq. 2 which satisfies no-slip boundary condition and maximum velocity (U_c) at the centreline. Uniform temperature T_{ref} = 300 K is used as thermal boundary condition at channel inlet.

$$u(y) = -4U_c\left[\left(\frac{y}{h}\right)^2 - \left(\frac{y}{h}\right)\right] \tag{2}$$

At the outlet boundary, pressure is set to zero, velocity and temperature gradients are also held at zero since the downstream length of the channel is sufficiently long as suggested by Valencia and Hinojosa (1997) to ensure fully developed laminar flow. Channel walls are treated as stationary with no-slip boundary condition. The upper wall together with the vertical and horizontal edges of the step are treated as adiabatic walls where the lower horizontal wall has a constant surface temperature of T_H = 350K. Boundary conditions for the BFS are shown in details in Fig. 1.

Three jets located around the step are denoted by the capital letters on the Fig. 2 as A, B and C, respectively. Jet A and C are at a distance h from the step wall while jet B is located in the middle of the step. Widths of all three jets are selected as w=0.073 h as suggested by Oyakawa *et al.* (1995) and Kiwan (2008).

Constant velocity value in normal direction is assigned for each jet boundary. The ratio of jet velocity to mean inlet velocity is named as jet velocity ratio. The positive values of jet velocity ratios indicate that the fluid is injected into the control volume while the negative values denote the fluid is sucked out of control volume. If the jet velocity ratio is equal to zero, wall with no-slip boundary condition is imposed at the corresponding
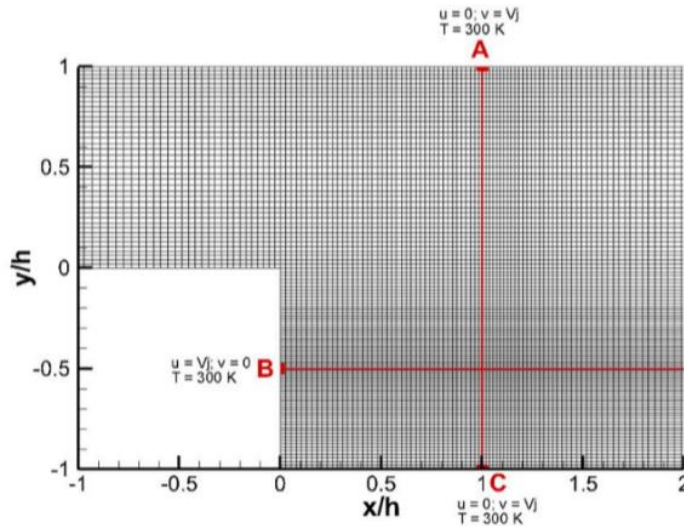
Fig. 2. The computational domain near the backward-facing step with three jet locations.

jet location. The jet velocity ratios are arranged in a way that the sum of all would be zero which is called Zero-Net-MassFlux system. The jet temperature is kept at constant value of 300 K.

Velocity ratios of jets A, B and C are independent control variables and case is named after these velocity ratios in the form of Case (A,B,C). Investigated cases are determined according to two constrains which are as follows: sum of all jet velocity ratios is zero (ZNMF) and each jet velocity ratio is in the range of -2 to 2. ZNMF condition reduces the number of independent parameters from three to two since the third jet velocity ratio C is linearly dependent on first two jets A and B. Five levels [-2, -1, 0, 1, 2] for each jet velocity ratio are determined.

Every combination of two control parameters with five levels result in 25 individual cases. In six cases out of 25, velocity ratio of jet C remained outside the defined limits of -2 and 2. Thus, remaining 19 cases are selected to be examined numerically.

While the velocity ratios of Jet A and B are independent control variables, average Nusselt number, skin friction coefficient, recirculation zone length, Strouhal number and amplitude of resulting oscillations are dependent variables which quantify hydrodynamic and thermal aspects of the flow problem. The primary aim of this study is to show the performance of chosen active control strategy by showing the changes in these dependent variables and commenting about the finer details of the evaluated results. Secondary goal is to increase the Nu number, since the most common interest in streaming work over a BFS is to increase heat transfer from the bottom wall.

2.1 Governing Equations and Solver Settings

A standard OpenFOAM solver 'buoyantBoussi-nesqPimpleFoam' is employed, since the flow investigated in this numerical study is unsteady, incompressible with un-negligible buoyancy.

Conservation of mass, momentum and energy equations for laminar flow with Boussinesq approximation are given in Eqs. (3), (4), (5) and (6), respectively.

$$\nabla \cdot \mathbf{u} = 0 \tag{3}$$

$$\frac{\partial \mathbf{u}}{\partial t} + \nabla \cdot (\mathbf{u}\mathbf{u}) = -\frac{1}{\rho_{ref}}(\nabla p - \rho g) + \nabla \cdot (\nu \nabla \mathbf{u}) \tag{4}$$

$$\rho = \rho_{ref}\left[1 - \beta(T - T_{ref})\right] \tag{5}$$

$$\frac{\partial T}{\partial t} + \nabla \cdot (T\mathbf{u}) = \nabla \cdot \left(\frac{\nu}{Pr}\nabla T\right) \tag{6}$$

The tolerance for all variables are selected as 1e-6 and for PIMPLE Algorithm, *number of outer correctors* and *number of correctors* are set equal to 50 and 3 respectively. Relaxation factors are kept as 1. Other constants and details of solver settings are summarized in Table 1.

2.2 Mesh and Time-Step Resolution Tests

In an early phase of this study, a mesh and time step size dependency test was conducted on an arbitrarily selected case. After all the cases simulated, it is observed by the authors that fluctuations occur when air is injected from jet C with a velocity ratio of 2 thus, flow becomes periodic. In order to capture these fluctuations with good accuracy, a secondary, more extensive mesh and time step dependency test was carried out since the flow is more dependent to these model parameters. $Case(-1,-1,2)$ is selected for this verification tests where the velocity fluctuations are strongest and $Re = 600$, $\Delta T = (T_H - T_{ref}) = 250K$ is used to cover a wider range of flow conditions for planned future studies, too. A critical point inside the flow field located at (5h,0) is selected to monitor transient variations of flow variables such as velocity components, pressure and temperature to investigate the dependency of numerical solution on the mesh and time step sizes.
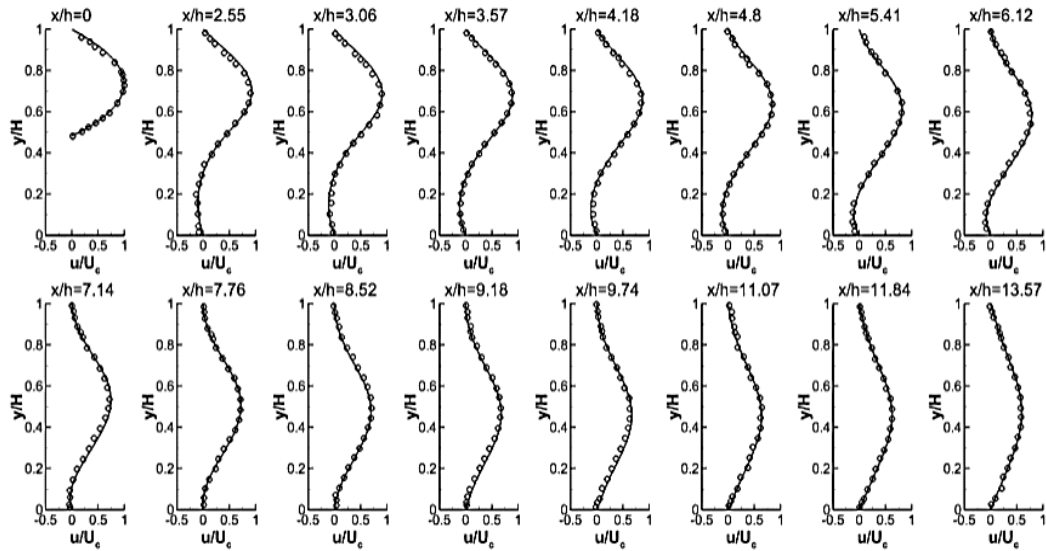
Fig. 3. Comparison of velocity profiles taken at various downstream positions for Re = 389, Case(0,0,0) with experimental data obtained from Armaly *et al*. Continuous lines represent the current study and the circles denote experimental data.

Table 1 Computational Settings

Transport Properties		Finite Volume Schemes		Solver and Smoothers		
$\nu = 1.502 \times 10^{-5}$	m^2/s	ddtScheme	Euler	Variable	Solver	Smoother
$\beta = 3.348 \times 10^{-3}$	1/K	gradScheme	Gauss Linear	p	GAMG	DIC Gauss Seidel
$T_0 = 300$	K	divScheme	Bounded Gauss Upwind	U,T	GAMG	Gauss Seidel
$Pr = 0.712$	-	laplacianScheme	Gauss Linear Corrected			
		interpolationScheme	Linear			

Spectral analysis is applied using fast Fourier transform (FFT) for x-component of velocity monitored at a selected point (x=5h, y=0) in flow domain and magnitude response is investigated for all cases. The highest magnitude and corresponding frequency obtained from FFT results are stored for each case. In the mesh and time step dependency tests, in addition to the time averaged x-velocity at that point, peak oscillation magnitude and corresponding frequency are also taken into consideration. Figure 4 (a) and (b) show the effects of time step and mesh size, respectively.

Meshes are refined in both x- and y-directions and clustered near wall boundaries and step region where the jets are located. It can be concluded from Fig. 4, the independence of the mesh and the time step size is achieved at 39488 number of cells and Δt = 0.000125 s, respectively, where the change in time averaged u, u-fluctuation magnitude and frequency is all lower than the selected tolerance of 5%. All cases are converged to an either steady or a periodic solution under 10 seconds. The simulations are performed until 15 s to obtain a time averaged solution calculated for each case from 101 instantaneous flow fields with a constant interval
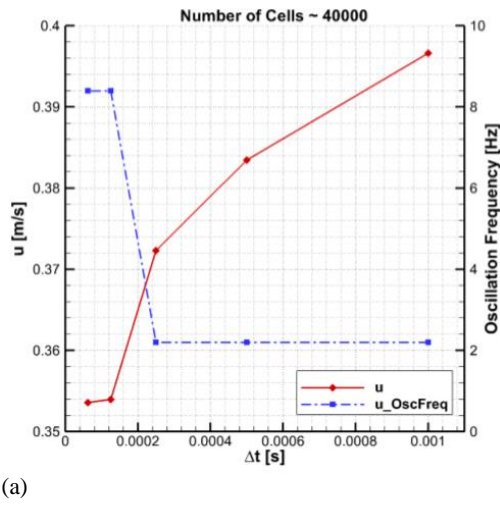
between 10-15 s.

Armaly *et al.* (1983) have experimentally shown that the span-wise velocity profile is almost uniform for Re up to 400. Armaly *et al.* (1983), Biswas *et al.* (2004) and Erturk (2008) have shown in their studies, a laminar BFS flow up to Re=400 can be reduced to a 2D problem. A test case for inlet Reynolds number of 389 is solved under isothermal conditions to validate the current 2D numerical results using verified mesh and time step. Velocity profiles downstream of the channel are compared to the experimental data obtained from the study of Armaly *et al.* (1983). A close agreement is achieved between the measurements and the current study as shown in Fig. 3. Among these profile comparisons, average and maximum root mean square error is calculated as 0.0259 and 0.0428, respectively.
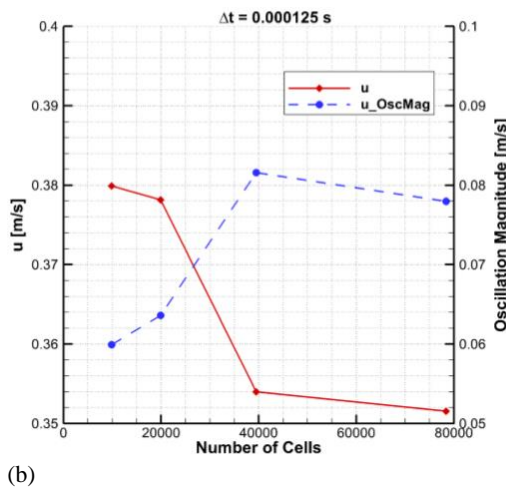
3. RESULTS AND DISCUSSION

After extensive grid and time step dependency tests along with validation of the results against the literature, all 19 cases described in previous sections are solved using the decided mesh and time step. The

variation of C_f and Nu along the bottom wall for 20 h are integrated and the total length of the recirculation zones are calculated for all cases.

$$C_f = \frac{\tau_w}{\frac{1}{2}\rho U_m^2} \qquad (7)$$

$$C_f = \frac{2\upsilon}{U_m^2}\left(\frac{\partial u}{\partial y}\right)\Bigg|_{wall} \qquad (8)$$

$$Nu = \frac{h_{air}D_H}{k} \qquad (9)$$

$$Nu = \frac{D_H}{\Delta T}\frac{\partial T}{\partial y}\Bigg|_{wall} \qquad (10)$$

The red zones of Nu and C_f represent the most effective cases indicating heat transfer enhancement and higher resistance to flow separation, respectively. Even though the most and the least effective regions can be seen, Fig.5 does not explain the physical causes behind the results obtained. Recirculation zone length, temporal variation of flow variables, time-averaged velocity and temperature contour plots are investigated and discussed in the following sections for further examination of this issue.

(a)

(b)

Fig. 4. (a) Time step and (b) mesh size dependency test results for Re=600, ΔT=250 K, Case (-1,-1,2).

In this study, C_f and Nu numbers along the bottom wall are selected as the dependent variables of interest. It is desired to increase these integral values in order to increase mixing and to reduce the total length of the recirculation zone. There are two input parameters that affect these variables which are velocities of jets A and B where velocity of jet C is linearly dependent to A and B due to ZNMF condition. Jet to inlet velocity ratios are kept as integers and between -2 and 2. As a result of these selected input parameters and constrains, operating range takes hexagonal shape. Figure 5 shows the interpolated contour plots of C_f and Nu numbers obtained from the time-averaged flow fields of all 19 cases each having unique jet velocity configuration.

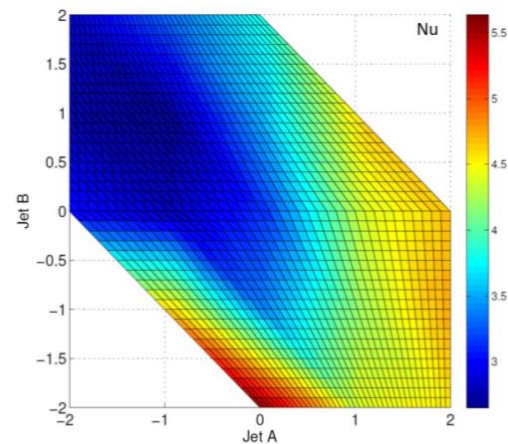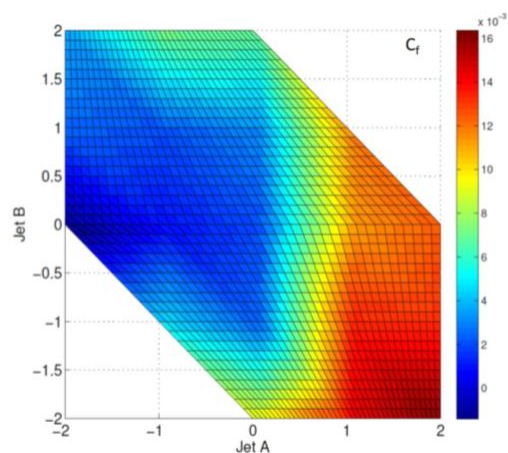The definitions of C_f and Nu are given in Eq. (7) to 10, respectively.

(a)

(b)

Fig. 5. Contour plots of (a) Nu and (b) C_f, interpolated from 19 cases.
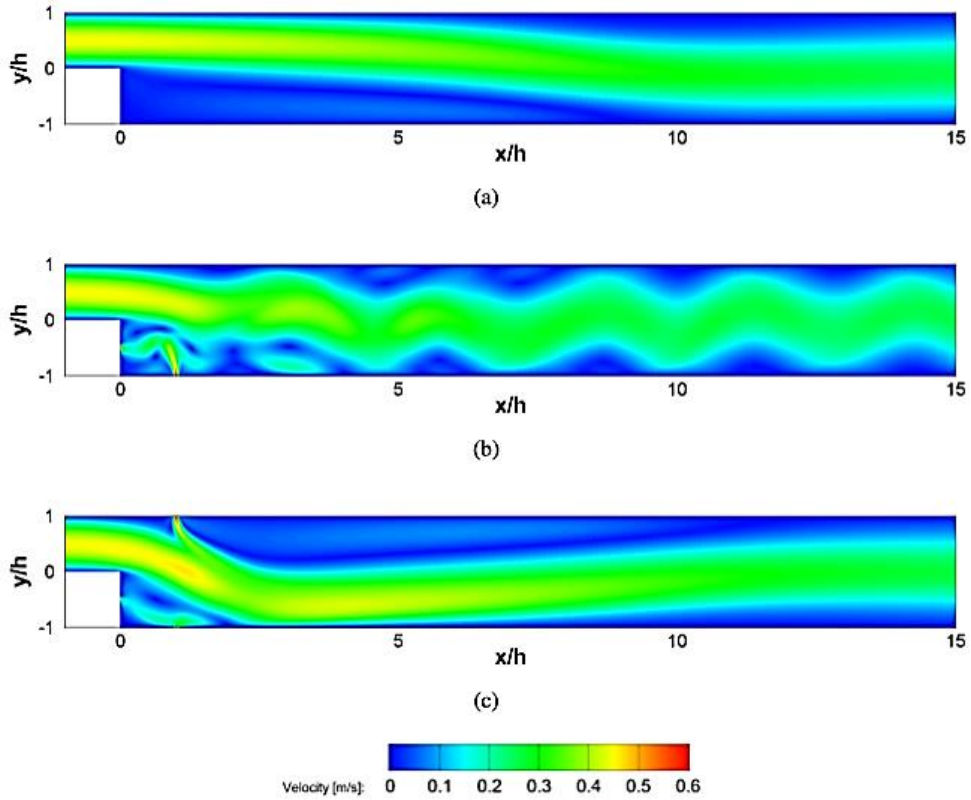
Fig. 6. Absolute velocity magnitude contours of averaged flow fields of (a) Case (0,0,0), (b) Case(0,-2,2) and (c) Case(2,-1,-1).
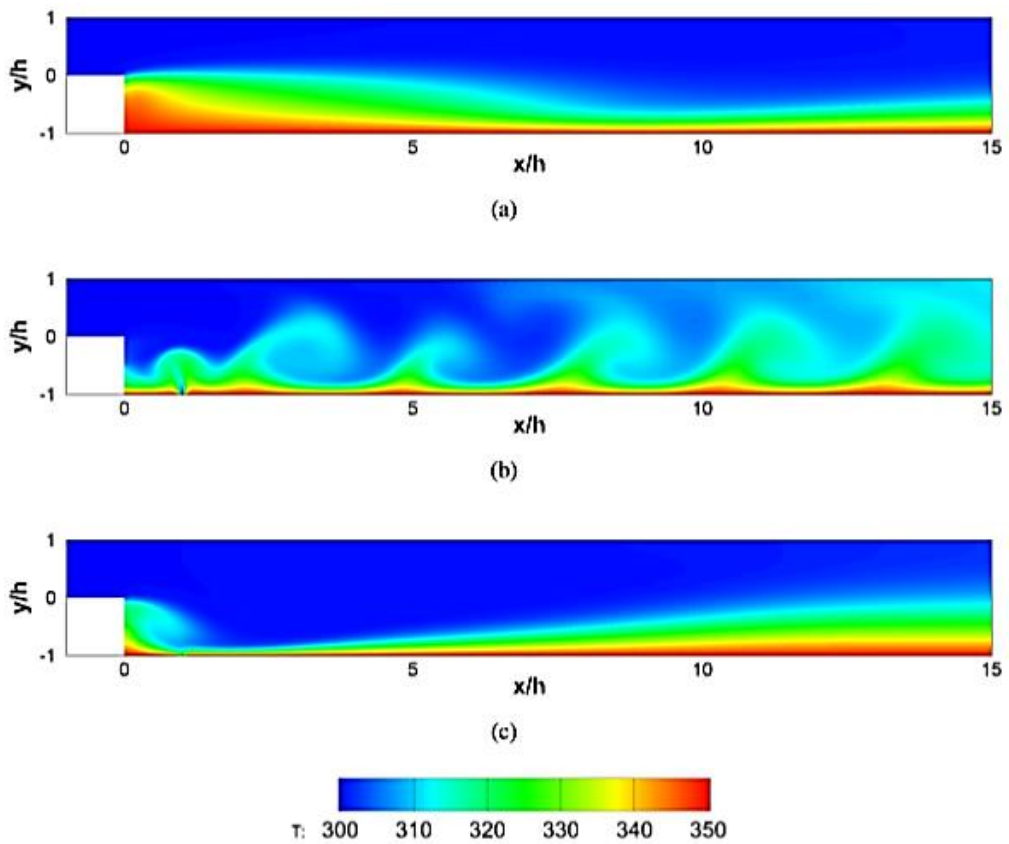

Fig. 7. Temperature contours of averaged flow fields of (a) Case (0,0,0), (b) Case(0,-2,2) and (c) Case(2,-1,-1).

3.1 Calculation of Total Recirculation Zone Length

The flow from inlet section separates on the BFS and reattaches with the bottom wall again after a certain distance. The pockets of circulating fluid created by this flow separation is called recirculation zone. These zones can be noticed on the velocity contours of averaged flow fields from selected cases shown in Fig.6. The total length of recirculation zone is calculated by the total length of bottom wall where C_f (x) takes negative values. Recirculation zones act as insulation regions between cold fluid coming from inlet and hot surface as can be seen in temperature contours given in Fig.7.

As it can be seen in Fig. 6 for the reference case of Case (0,0,0) where no flow control is applied, the recirculation zone length is calculated as 9 h . In Fig. 6b it is shown that with the use of chosen active flow control strategy, recirculation zone length is reduced up to 1.73 h on Case(2,-1,-1). However Case (0,-2,2) results in multiple recirculation zone. In Fig. 8 Nu and C_f variation along the bottom wall are compared on selected cases.
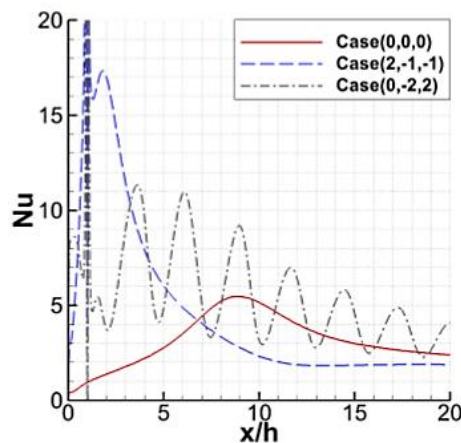
(a)
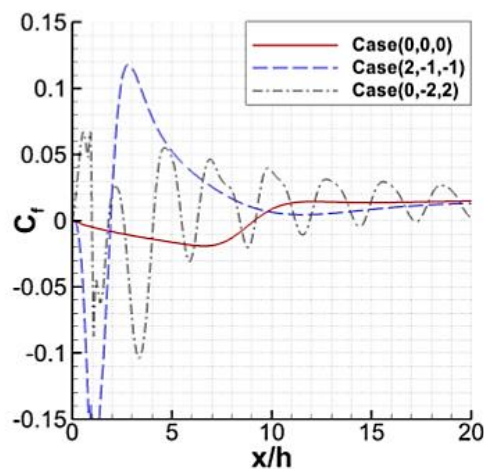
(b)

Fig. 8. (a) Nu and (b) C_f variation along bottom wall for 20 h.

The cases with reduced recirculation region, convective heat transfer is enhanced due to better mixing of the cold fluid with the heated fluid near the bottom wall, which results in a considerably increased averaged Nu along the bottom wall. Total normalized recirculation zone length of all cases are shown in Fig. 9.

In general, the total recirculation zone reduces at the positive jet velocity ratio of A, as it can be seen from Fig. 9. It is also expected that for the cases where the recirculation zone is smaller, Nu is higher since recirculation zones act as insulation areas. This effect can be seen in Fig. 5a and 5b. Even though this assumption is true for most of the cases, the highest Nu is achieved at Cases (0,-2,2) and (1,-1,2) where both result with multiple recirculation bubbles. This result contradicts with the general assumption and it is explained in details by temporal investigation. Figure 10 shows the x-velocity fluctuations monitored at 5h distance from the BFS obtained from frequency spectrum analysis.
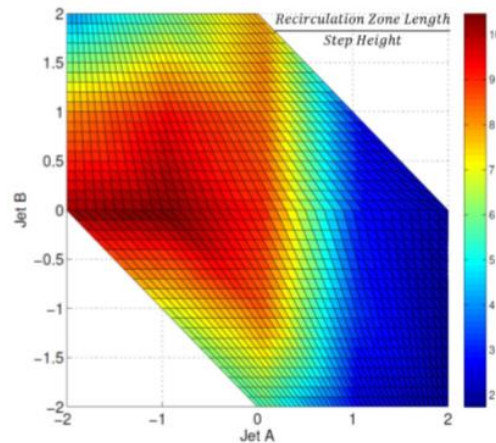

Fig. 9. Interpolated total recirculation zone length contours, normalized with step height h.

In most of the configurations, the flow converges to a steady-state solution however, for the cases where jet C has high positive velocity ratio of 2, flow becomes periodic. It is observed that when flow is periodic, Nu is substantially high compared to steady cases even though the total recirculation zone length is high. This issue is explained with the fact that excitation becomes periodic due to jet and base flow interaction which leads to enhanced mixing, even though the jet flow rates are constant and steady. In Fig. 5a and 10b it is shown that Nu is increased, mixing of cold and heated fluids is enhanced as the fluctuation magnitude increases. In Fig. 11, the decay of the magnitude of velocity component fluctuations are shown for Case (0,2,2) where the highest fluctuation magnitude is observed. It can be seen that the magnitude of vertical velocity fluctuation is still existing near the outlet of the channel which suggests a better mixing for larger portion of the flow field. This effect can also be seen in Fig. 8a where fluctuating Nu variation along the bottom wall is higher for larger portion of the wall compared to other configurations.

Table 2 Summary of overall results

| Jet A	Jet B	Jet C	C_f	Nu	RZL/h	St[u(x=5h,y=0)]	OscMag[u(x=5h,y=0)] [m/s]
-2	0	2	-1.40E-03	3.02	10.20	0.25	3.31E-03
-2	1	1	2.35E-03	2.71	8.20		
-2	2	0	3.51E-03	2.83	4.20		
-1	-1	2	4.73E-03	4.69	6.73	0.21	2.22E-02
-1	0	1	8.40E-04	2.80	10.47		
-1	1	0	2.02E-03	2.65	9.33		
-1	2	-1	6.95E-03	3.28	5.87		
0	-2	2	9.62E-03	5.64	5.47	0.18	4.43E-02
0	-1	1	2.48E-03	3.42	8.40		
0	0	0	1.96E-03	3.16	9.00		
0	1	-1	3.08E-03	3.57	8.40		
0	2	-2	6.80E-03	3.83	7.93		
1	-2	1	1.44E-02	4.43	2.40		
1	-1	0	1.35E-02	4.23	3.13		
1	0	-1	1.13E-02	4.36	2.87		
1	1	-2	1.20E-02	4.63	2.67		
2	-2	0	1.64E-02	4.56	1.73		
2	-1	-1	1.34E-02	4.77	1.73		
2	0	-2	1.25E-02	4.69	1.87		

(a)　　　　　　　　　　　　　　　　　(b)
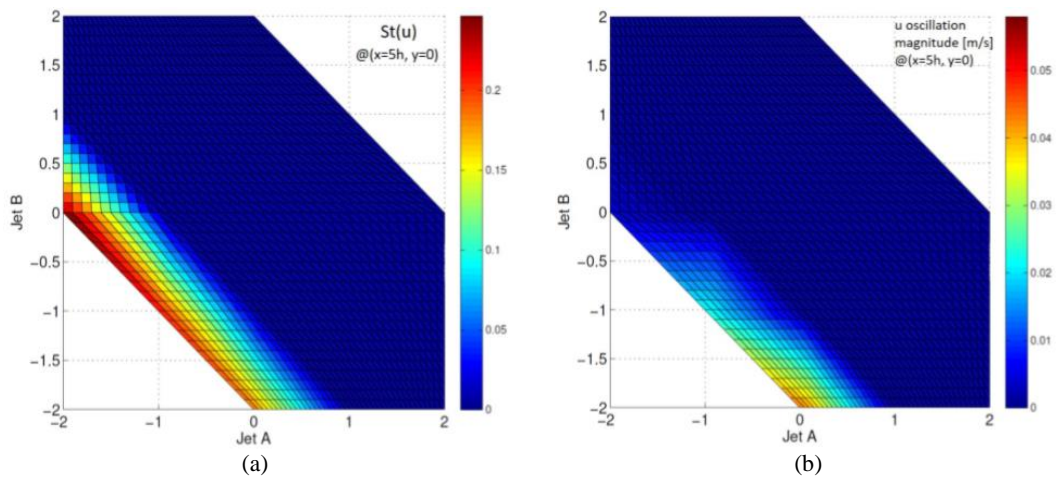
Fig. 10. Interpolated (a) Strouhal number and (b) fluctuation magnitude of u velocity contours.

Figure 12 shows dimensionless temperature and uvelocity profiles extracted from time averaged flow fields of the selected cases at x = 6 h. Active flow control on the hydrodynamic and thermal boundary layers are evaluated by the velocity and temperature gradients which are directly related to C_f and Nu. Highest velocity gradient is achieved for Case (2,-1,-1) where flow separation is completely prevented. However for the Case (0,-2,2) there is a slight back flow which shows that a steady state C_f decay is better than a periodic C_f in terms of flow separation control. The most effective thermal boundary layer control is achieved at the Case (0,2,2) since the temperature gradient is highest due to the periodic character of the Nu variation along the bottom wall as can be seen in Figure 12. Table 2 summarizes the average value of investigated dependent variables along the bottom wall for the length of 20h calculated from time averaged flow fields. As it can be seen from Table 2 three cases converged to a periodic solution and for only these three cases maximum u-velocity oscillation magnitude and corresponding St numbers are indicated. Blank cells denote cases which yield steady state solutions.
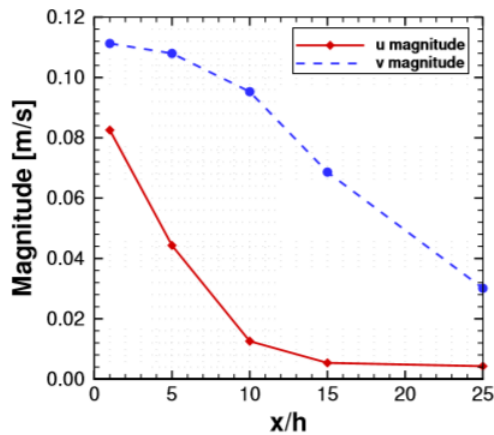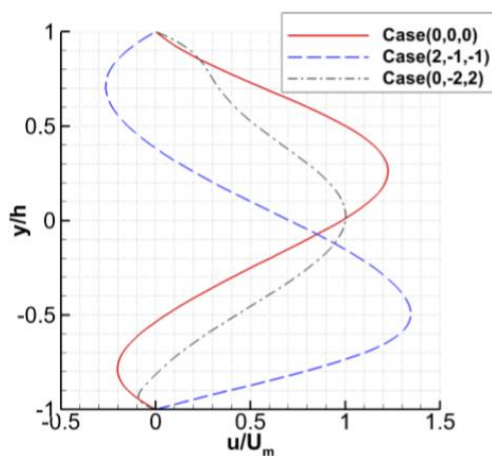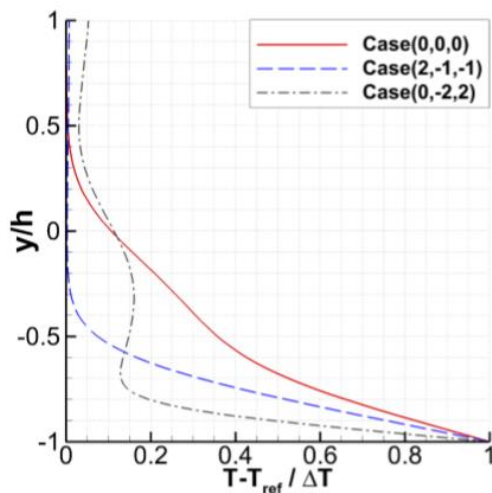
Fig. 11. Decay of fluctuation magnitudes in stream-wise direction for Case (0,-2,2).

(a)

(a)

Fig. 12. Dimensionless (a) u-velocity, (b) temperature.

4. CONCLUSION

In this study, fluid flow and heat transfer over a BFS is numerically investigated by using OpenFOAM. An active flow control is applied by means of local suction and injection from three thin slits distributed around the step to enhance the heat transfer rate. In this context, the performance of 19 ZNMF configurations are tested for inlet Reynolds number of 400 after extensive mesh, time step dependency tests and validation by available experimental measurements in literature have been carried out. The C_f, Nu, St, velocity oscillation magnitude and total recirculation zone length along the bottom wall are calculated for each case and plotted to visualize their variation as jet configuration changes. Velocity and temperature contours generated from time averaged flow fields, velocity and temperature profiles at selected downstream locations of several representative cases are compared to the reference case in which the flow control is not applied. It is concluded that injection from the upper wall is more effective to increase Nu compared to the other jet configurations. However, it is also shown that injection from the lower wall at high velocities causes oscillations inside the flow field which increases Nu due to better mixing. The most promising cases in the present study resulted in an increase of 78.5\% in the average Nu along the bottom wall and reduction of 81\% of the total recirculation zone length compared to reference case with no flow control is applied.

REFERENCES

Ahmed, H. E., A. S. Kherbeet, M. I. Ahmed and B. H. Salman (2018). Heat transfer enhancement of micro-scale backward-facing step channel by using turbulators. *International Journal of Heat and Mass Transfer* 126, 963–973.

Ahmed, K., M. Ali and F. Alvi (2014). Mixing Characteristics of Active Microjet-Based Actuators in a Supersonic Backward-FacingStep Flow. *AIAA Journal* 52(12), 2855–2866.

Al-Aswadi, A. A., H. A. Mohammed, N. H. Shuaib and A. Campo (2010). Laminar forced convection flow over a backward facing step using nanofluids. *International Communications in Heat and Mass Transfer* 37(8), 950–957.

Anguraj, A. and J. Palraj (2018). Numerical study of fluid flow and heat transfer in a backward facing step with a rotating cylinder. *Malaya Journal of Matematik* 06(02), 435–442.

Armaly, B. F., F. Durst, J. C. F. Pereira and B. Schonung (1983). Experimental and theoretical investigation of backward-facing step flow. *Journal of Fluid Mechanics* 127, 473–496.

Bayraktar, S. (2014). Numerical solution of three-dimensional flow over angled backward-facing step with raised upper wall. *Journal of Applied Fluid Mechanics* 7, 155–167.

Biswas, G., M. Breuer and F. Durst (2004, 07). Backward-Facing Step Flows for Various Expansion Ratios at Low and Moderate Reynolds Numbers. *Journal of Fluids*

Engineering 126(3), 362–374.

Bouterra, M., Z. Mehrez, A. E. Cafsi, A. Belghith and P. Quere (2011). Control of local mass transfer in the separated and reattaching flow by a periodic forcing. *Journal of Applied Fluid Mechanics* 4, 63–67.

Chovet, C., M. Lippert, L. Keirsbulck and J. M. Foucaut (2016). Dynamic characterization of piezoelectric micro-blowers for separation flow control. *Sensors and Actuators, A: Physical* 249, 122–130.

Chovet, C., M. Lippert, L. Keirsbulck and J. M. Foucaut (2019). Unsteady Behavior of a Backward-facing Step in Forced Flow. *Flow, Turbulence and Combustion* 102(1), 145–165.

Chun, K. B. and H. J. Sung (1996). Control of turbulent separated flow over a backward-facing step by local forcing. *Experiments in Fluids* 21(6), 417–426.

Dandois, J., E. Garnier and P. Sagaut (2007). Numerical simulation of active separation control by a synthetic jet. *Journal of Fluid Mechanics* 574, 25–58.

Dejoan, A., Y.-J. Jang and M. A. Leschziner (2005, 03). Comparative les and unsteady rans computations for a periodically-perturbed separated flow over a backward-facing step. *Journal of Fluids Engineering* 127(5), 872–878.

Emami-Naeini, A., S. McCabe, D. D. Roover, J. Ebert and R. Kosut (2005). Active Control of Flow Over a Backward-Facing Step. *Proceedings of the 44th IEEE Conference on Decision and Control*, 7366–7371.

Erturk, E. (2008). Numerical solutions of 2-d steady incompressible flow over a backward-facing step, part i: High reynolds number solutions. *Computers and Fluids* 37(6), 633 – 655.

Gad-el Hak, M. (2006). *Flow control: passive, active, and reactive flow management* (Digitally printed 1st pbk. version ed.). Cambridge: Cambridge University Press.

Giachetti, B., M. Fénot, D. Couton and F. Plourde (2018). Influence of multiperforation synthetic jet configuration on heat transfer enhancement. *International Journal of Heat and Mass Transfer* 125, 262–273.

Kanchi, H. and F. Mashayek (2012, 07). Effects of microjets in flow over a backward-facing step. *Engineering Systems Design and Analysis Volume 2: Applied Fluid Mechanics; Electromechanical Systems and Mechatronics; Advanced Energy Systems; Thermal Engineering; Human Factors and Cognitive Engineering*, 83–89.

Kapiris, P. G. and D. S. Mathioulakis (2014). Experimental study of vortical structures in a periodically perturbed flow over a backward-facing step. *International Journal of Heat and*

Fluid Flow 47, 101–112.

Khanafer, K., B. Al-Azmi, A. Al-Shammari, and I. Pop (2008). Mixed convection analysis of laminar pulsating flow and heat transfer over a backward-facing step. *International Journal of Heat and Mass Transfer* 51(25-26), 5785–5793.

Kim, S., H. Choi and J. Y. Yoo (2007). Effect of local forcing on backward-facing step flow with laminar separation. *Journal of Turbulence* 8(June), 1–23.

Kiwan, S. (2008). Using localized wall discharge to control the fluid flow and heat transfer for the flow over a backward facing step. *International Journal of Numerical Methods for Heat & Fluid Flow* 18(6), 745– 765.

Kumar, S. and S. Vengadesan (2018). Control of separated fluid flow and heat transfer characteristics over a backward facing step. *Numerical Heat Transfer; Part A: Applications* 73(6), 366–384.

Li, Z. Y., S. Guo, H. L. Bai and N. Gao (2019). Combined flow and heat transfer measurements of backward facing step flows under periodic perturbation. *International Journal of Heat and Mass Transfer* 130, 240–251.

Lin, J., B. Armaly and T. Chen (1990). Mixed convection in buoyancy-assisting, vertical backward-facing step flows. *International Journal of Heat and Mass Transfer* 33(10), 2121 – 2132.

Mehrez, Z., M. Bouteraa, A. Elcafsi, A. Belghith and P. Le Quéré (2010). Active Control of Flow Behind a Backward Facing Step by Using a Periodic Perturbation. *ARPN Journal of Engineering and Applied Sciences*, 21–29.

Mehrez, Z., M. Bouterra, A. E. Cafsi, A. Belghith and P. L. Quéré (2010). Simulation of the Periodically Perturbed Separated and Reattaching Flow over a Backward-Facing Step. *Journal of Applied Fluid Mechanics* 3, 1–8.

Mehrez, Z., M. Bouterra, C. A. El, A. Belghith and Q. P. Le (2011). Mass transfer control of a backward-facing step flow by local forcing-effect of Reynolds number. *Thermal Science* 15(2), 367–378.

Nait Bouda, N., R. Schiestel, M. Amielh, C. Rey and T. Benabid (2008). Experimental approach and numerical prediction of a turbulent wall jet over a backward facing step. *International Journal of Heat and Fluid Flow* 29(4), 927–944.

Okada, K., K. Miyaji, K. Fujii, A. Oyama, T. Nonomura and K. Asada (2010). Computational study of the synthetic jet on separated flow over a backward-facing step. *ASME 2010 International Mechanical Engineering Congress and Exposition* 7(1), 161– 170.

Oyakawa, K., T. Taira, I. Senaha, T. Nosoko and M. Hiwada (1995). Heat transfer control by using jet discharge in reattachment region downstream of a backward-facing step. *International Communications in Heat and Mass Transfer* 22(3), 343–352.

Rhee, G. H. and H. J. Sung (2000). Enhancement of heat transfer in turbulent separated and reattaching flow by local forcing. *Numerical Heat Transfer; Part A: Applications* 37(7), 733–753.

Takano, S., M. Momotsuke and S. Honami (2014). A study on backward facing step flow in low reynolds number manipulated by synthetic jets - effect of different jet velocities -. *Journal of Fluid Science and Technology* 9(3).

Tihon, J., V. Pěnkavová and M. Pantzali (2010). The effect of inlet pulsations on the backward-facing step flow. *European Journal of Mechanics, B/Fluids* 29(3), 224–235.

Uruba, V., P. Jonáš and O. Mazur (2007). Control of a channel-flow behind a backward-facing step by suction/blowing. *International Journal of Heat and Fluid Flow* 28(4), 665–672.

Valencia, A. and L. Hinojosa (1997). Numerical solutions of pulsating flow and heat transfer characteristics in a channel with a backward-facing step. *Heat and Mass Transfer* 32(3), 143–148.

Velazquez, A., J. R. Arias and B. Mendez (2008). Laminar heat transfer enhancement downstream of a backward facing step by using a pulsating flow. *International Journal of Heat and Mass Transfer* 51(7-8), 2075– 2089.

Wengle, H. and A. Huppertz (2001). The manipulated transitional backward-facing step flow: an experimental and direct numerical simulation investigation. *European Journal of Mechanics B Fluids* 20, 25–46.

Xu, F., Z. Gao, X. Ming, L. Xia, Y. Wang, W. Sun and R. Ma (2015). The optimization for the backward-facing step flow control with synthetic jet based on experiment. *Experimental Thermal and Fluid Science* 64, 94–107.

Yoshioka, S., S. Obi and S. Masuda (2001, 6). Organized vortex motion in periodically perturbed turbulent separated flow over a backward-facing step. *International Journal of Heat and Fluid Flow* 22(3), 301–307.

Zhao, L. and M. Dong (2020). Effect of suction on laminar-flow control in subsonic boundary layers with forward-/backward-facing steps. *Physics of Fluids* 32(5).